Diameter assessment of soilcrete column using in-hole electrical resistivity tomography

CHUN-HUNG LIN*, CHIH-PING LIN†, YIN JEH NGUI†, HAORAN WANG‡, PO-LIN WU†, GUAN-JIE HE† and HSIN-CHANG LIU†

Quality control of jet grouting at large depth is a challenging task. An in-hole electrical resistivity method was recently shown to have high potential for assessing the diameter and integrity of jet grouting. To facilitate visualised inspection and practical use of the in-hole resistivity method for jet grouting, this study introduces a novel and practical tomographic approach. An analogous mapping approach from axially symmetric in-hole electrical resistivity tomography (ERT) to two-dimensional (2D) half-space surface ERT is proposed, allowing direct implementation of widely available 2D inversion software. A quantitative reduction method is also proposed to determine accurately the variation of column diameter from the inverted tomogram. Numerical simulations validate the proposed approach and show that the estimation error is within 10% when the electrode spacing is less than 1/5 of the column diameter. The spatial resolution and the effect of axially asymmetric condition are numerically investigated, the latter suggesting the importance of centralising electrodes in the soilcrete column. Two physical model tests are performed and verify the performance of the proposed method experimentally.

KEYWORDS: geophysics; ground improvement

INTRODUCTION

High-pressure jet grouting is a commonly used ground improvement technique to enhance in situ ground competence. Several applications in geotechnical engineering can be found in the literature, for example, the cut-off wall (Croce & Modoni, 2005), tunnel (Croce *et al.*, 2004; Arroyo *et al.*, 2011; Burke, 2012), bottom plugs (Eramo *et al.*, 2012; Tan *et al.*, 2015), diaphragm wall (Hsieh *et al.*, 2003), foundations (Modoni & Bzówka, 2012) and so on.

The technique mainly channels cement grout suspensions with a high-pressure jet nozzle into surrounding soils, in order to cut through in situ soils and form a soilcrete column. Soilcrete columns are mixtures of grout and in situ soil formed within the cutting region, which is capable of improving the soil shear strength and the ground impermeability. The effectiveness of jet grouting improvement is highly dependent on the construction integrity of individual soilcrete columns. Owing to construction uncertainties or possible negligence, insufficient radius or even discontinuous soilcrete may occur. These unfavourable anomalies may prevent a post-improvement site from achieving the targeted design goal. Quality control (QC) of soilcrete columns is therefore crucial and necessary for ensuring the overall construction quality.

The dimensions and integrity of soilcrete columns are the main QC factors in jet grouting. Although empirical approaches (Flora & Lirer, 2011; Ochmański *et al.*, 2015; Tinoco *et al.*, 2016) or theory-based models (Modoni *et al.*, 2006; Wang *et al.*, 2012; Flora *et al.*, 2013) considering injection parameters and soil shear strength are available for estimation of the average dimension, independent inspections are still necessary. Jet grouting QC is conventionally assessed by visual inspection at shallow depths and soilcrete core sampling at large depths. These QC methods are time consuming and cost ineffective. Only a small proportion of the site is tested to evaluate the construction quality. Some indirect measurements have emerged, such as the hydrophone or painted bar approach (Kimpritis, 2013), which checks the erosion or vibration phenomenon at the vicinity of the designed column radius to determine whether the grouts have reached the designed radius. However, these tagged detection methods can only reveal that the jet grouts have reached the marked location, but the actual formation of cement grout remains unknown.

Following the development of geophysical methods, subsurface imaging techniques have been applied more recently to jet grouting inspections, for instance the downhole/surface seismic (Madhyannapu *et al.*, 2010), crosshole ultrasonic/seismic (Niederleithinger *et al.*, 2010; Bearce *et al.*, 2014; Spruit *et al.*, 2014; Guerreros *et al.*, 2016). The direct current (DC) resistivity method in particular is a powerful imaging approach in jet grouting inspection. The main advantage of the DC resistivity method is that it can delineate the region of soilcrete in the natural ground due to the significant difference in their typical resistivity values. The typical resistivity of soil lies within ten to several hundred Ω m depending on the soil type and pore water salinity, whereas the resistivity of soilcrete is typically within 1–7 Ω m even at the seventh day after placement (Liu *et al.*, 2007). Resistivity of fresh grout can be as low as 1–3 Ω m (Bearce *et al.*, 2016). These characteristics provided a good contrast between the soilcrete column and the surrounding soils, in favour of high-resolution assessment by resistivity method. Moreover, seismic measurements require at least 2 days of curing for the soilcrete to have sufficient stiffness to generate detectable and distinguishable signals. The DC resistivity method, on the other hand, allows immediate inspection of the soilcrete column (Bearce *et al.*, 2015; Mooney & Bearce, 2017).

Manuscript received 22 September 2018; revised manuscript accepted 3 September 2019.
Discussion on this paper is welcomed by the editor.
* National Sun Yat-sen University, Kaohsiung, Taiwan.
† National Chiao Tung University, Hsinchu, Taiwan.
‡ ST Geomative Co., Nanshan District, Shenzhen, P. R. China.

The DC resistivity method utilises four electrodes (as shown in Fig. 1), two of which (A and B in Fig. 1) inject direct current into the ground from a voltage source, while the other two (M and N in Fig. 1) measure the resulting ground electrical potential at some designated locations. Various four-electrode array configurations are available, such as Wenner, Wenner–Schlumberger, dipole–dipole, pole–dipole, pole–pole and gradient arrays. The choice of array type is related to considerations of vertical and horizontal sensitivity, investigation depth and signal strength. By varying the spacing and location of the four electrodes, data for different influence depths at different locations can be collected and used to invert for resistivity distribution (Loke, 1999). Depending on the layout of electrodes in the ground, the DC resistivity method can be categorised into surface electrical resistivity tomography (ERT), cross-hole ERT and in-hole (single-borehole) ERT. For inspecting a jet grout column, surface ERT suffers from insufficient spatial resolution in depth. Cross-hole ERT provides better depth resolution, but it is cost-ineffective because it requires at least two boreholes. A patented in-hole ERT technique called Cyljet (Frappin, 2011), a special application of the electric cylinder method (Frappin & Morey, 2001), appears to be the most appealing technique. Its in-hole measurement avoids the drawbacks associated with surface survey by using a single hole at the centre of the soilcrete column to lay out the in-hole electrode string. The testing procedure involves pushing a slotted polyvinyl chloride (PVC) pipe into the centre of the fresh grout or re-drilling the centre of the soilcrete after 1–2 days of curing for the in-hole DC resistivity measurements. In addition, a calibration hole can be drilled and equipped with the same slotted PVC pipe in the untreated ground to measure its natural background resistivity. The Cyljet method can generate a complete depth profile of soilcrete column diameter efficiently and cost-effectively. However, the lack of detailed survey provision and inversion methodology of this proprietary technique has limited its use in general engineering practice.

Based on a similar concept, Bearce *et al.* (2016) evaluated the applicability of the Wenner-α array with direct coupled electrodes and proposed a diameter estimation approach based on a numerical parametric study. Three-dimensional (3D) forward numerical simulation was the kernel of this approach. First, a homogeneous half-space was constructed to provide geometric factors for calculating apparent resistivities, accounting for the influence of surface boundary. The in-hole measurements (i.e. electrical current and potential for each array) were converted to apparent resistivities from these geometric factors. A relationship between column diameter and apparent resistivity was then numerically established by forward simulations using earth models with soilcrete columns of various diameters. This relationship was finally used for diameter assessment. Although this approach is feasible, it is cumbersome that the site-specific earth model in the 3D simulations should be constructed manually for each site; and the accuracy of diameter estimations relies on setting or estimating the appropriate resistivity values in the model. A true tomographic approach that inverts the measured apparent resistivity to obtain a resistivity section for direct quantitative interpretation is desirable. Besides, the result of in-hole resistivity measurements is a weighted average from all azimuths. The effect of an axially asymmetric column on such measurement should be examined.

In light of all of the above, the aim of the present study was to explore the feasibility of utilising a widely available two-dimensional (2D) Cartesian coordinate inversion system to perform ERT inversion of in-hole data for column diameter visualisation and estimation. 3D numerical simulations were performed to validate the proposed method and to investigate the spatial resolution and the effect of an axially asymmetric soilcrete column. Physical model tests were also performed for experimental validation.

METHODS

From axially symmetric to 2D Cartesian half-space

Figure 1(a) illustrates the electrical potential distribution during a current injection from two current electrodes (A and B) in a surface ERT. Since the air region above ground can be regarded as a non-conductive medium, the equipotential surface is perpendicular to the ground surface and is distributed underground in hemispherical shape in a homogeneous medium. The in-hole ERT transposes the electrode arrangement from the ground surface to a borehole

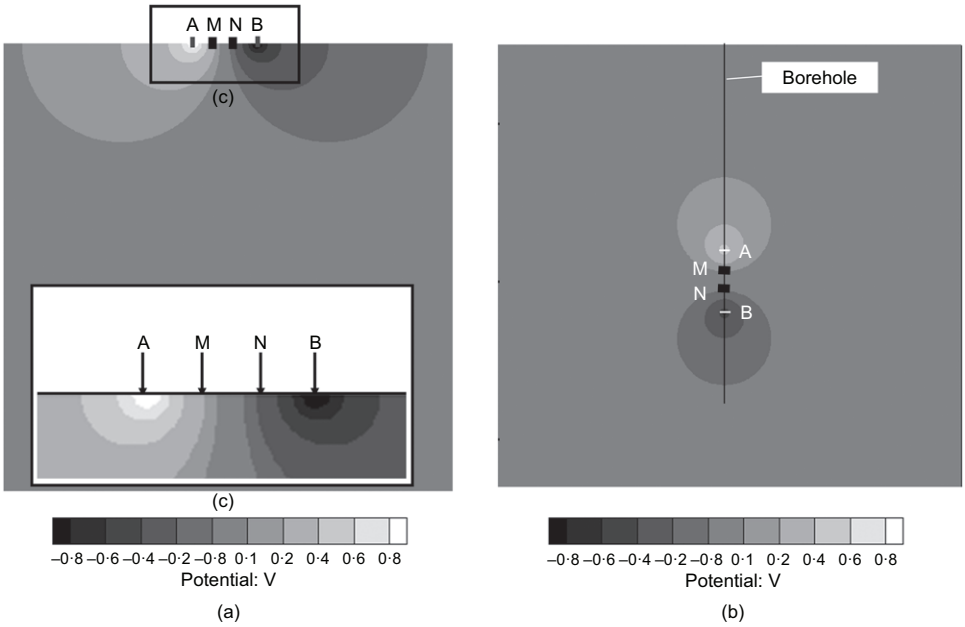

Fig. 1. Equipotential distribution during current injection from two current electrodes in (a) surface ERT and (b) in-hole ERT. (c) Close-up of (a) showing the current electrodes (A and B) and potential electrodes (M and N) in more detail

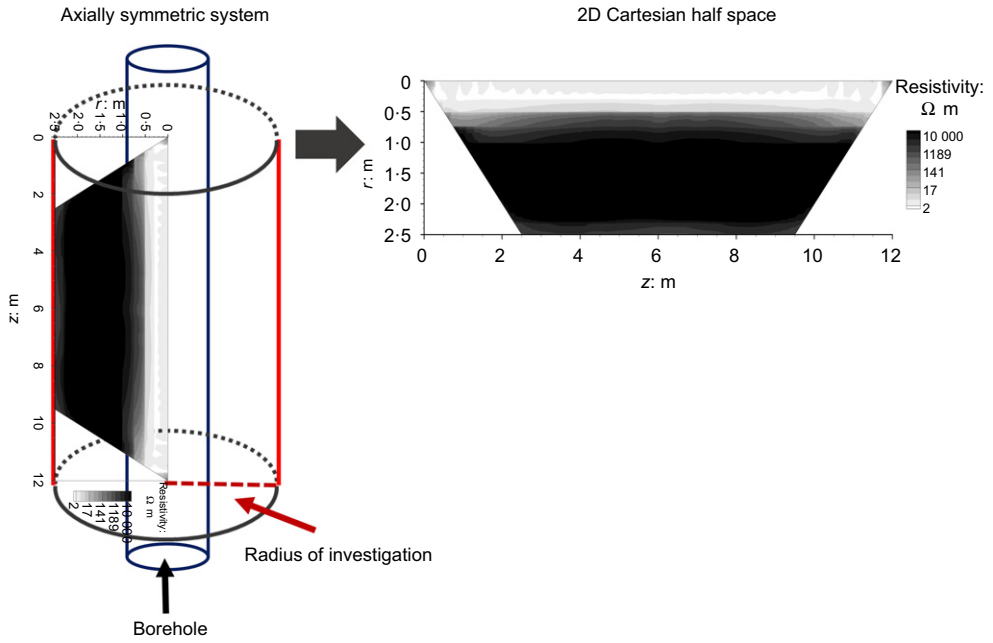

Fig. 2. Schematic representation of equivalency mapping from axially symmetric in-hole ERT to 2D half-space surface ERT

so that the resistivity of geomaterials surrounding the borehole can be measured. In a homogeneous medium, the electrical potential induced by an in-hole measurement is axially symmetric and perpendicular to the borehole in a way similar to the surface ERT, as shown in Fig. 1(b). This similarity suggests that 2D ERT in half-space is analogous to the axially symmetric in-hole ERT.

It is reasonable to assume an axially symmetric condition when in-hole ERT is used for jet grouting inspection. Therefore, inversion of in-hole ERT becomes a 2D problem. Inspired by the similarity in Fig. 1, the aim of the present study was to explore the feasibility of utilising a widely available 2D Cartesian half-space inversion software to perform ERT inversion of in-hole data for column diameter estimation, as illustrated in Fig. 2. When the axially symmetric condition is mapped to the 2D half-space, the radial direction of interest becomes the depth in the 2D half-space; and azimuthal homogeneity is represented by the homogeneity in the direction perpendicular to the survey line in two dimensions. In cases where soilcrete columns are not truly circular, the resistivity profile in the axially symmetric system is regarded as some weighted average in all azimuths. The proof of concept is given by numerical simulations and physical models elaborated as follows.

Numerical simulations and parametric studies

This study utilised the Comsol Multiphysics Version 4.4 (Comsol Multiphysics, 2013), a finite-element software capable of coupling multiple physical parameters, for forward modelling of the 3D electrical potential field during ERT measurements. By dynamically linking a self-compiled Matlab code to the Comsol forward model, various electrode arrays were prescribed to automatically compute the corresponding resistivity pseudo section, a representation of apparent resistivities measured by each four-electrode array. All boundaries were set as absorbing boundaries except for the surface of the model, which was set as a non-conductive boundary. The dimension of the numerical model is 20 m × 20 m × 27 m and the placement of simulated soilcrete is demonstrated in Fig. 3. Free tetrahedral meshing was used

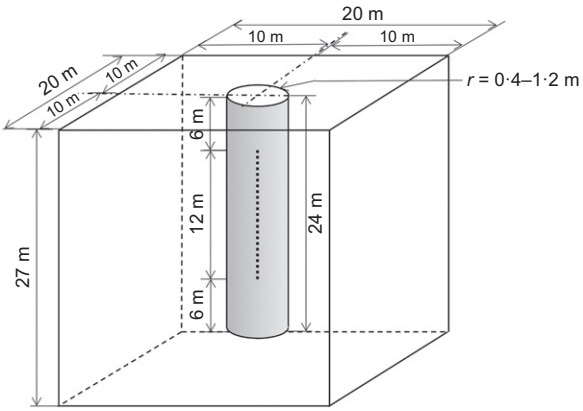

Fig. 3. Set-up of numerical models (not to scale)

with mesh size ranging from 0·08 m (near the survey line) to 0·8 m (in less sensitive regions). The simulated ERT data were acquired by 31 electrodes in a Wenner–Schlumberger array with a total of 402 quadrupoles. 2D half-space inversion of simulated data was performed by a commercial inversion software EarthImager 2D 2.4.4 (AGI, 2015). The smooth model inversion was adopted as the inversion method in the EarthImager 2D. Default inversion settings were used except for the starting model and the maximum number of iterations in the stopping criteria. Pseudo sections were used as the starting models for the 2D inversions, while the number of iterations was set to seven regardless of the root mean square (RMS) error and error reduction. The reason for forcing seven iterations in the inversion will be explained in the 'Results and Discussion' section later. It is also noted that the minimum and the maximum resistivity in the resistivity inversion was limited to 1 and 100 000 Ω m, respectively. The tomogram inversion process for both numerical simulation and experimental validation adopted the same inversion parameters and stopping criterions.

In order to evaluate the feasibility and applicability of the proposed method, in this study three types of soilcrete columns were designed, namely, the intact columns with various radii, columns with symmetrical defects (i.e. necking)

or changing diameter and columns with asymmetrical defects. Numerical simulations were performed by placing an individual soilcrete column in a homogeneous half-space representing the soil. Previous studies (Bearce *et al.*, 2016; Liu *et al.*, 2007) show that the resistivity of jet grout (1–7 Ω m) is lower than typical natural soils. The resistivity of the soilcrete column and the background soil was assumed as 5 Ω m and 50 Ω m, respectively. The resistivity values of soilcrete and soil are site dependent; the reference values adopted in numerical simulations are to ensure that the required resistivity contrast suggested by Frappin & Morey (2001) is met. Although there could be other situations in which resistivity of soilcrete is higher than ground resistivity, a more typical condition is considered here for method development. The in-hole ERT survey line was located at the centre of the soilcrete column to simulate the direct coupling between electrodes and soils. The in-hole ERT electrode spread is 12 m long with the uppermost electrode at 6 m below the ground level, as shown in Fig. 4; 31 electrodes were deployed with the electrode spacing of 0·4 m. For good sensitivity in both radial and axial directions, a Wenner–Schlumberger array (Loke, 1999) was adopted in this study.

Physical model

In addition to the numerical verification and investigation, two physical models were designed to experimentally validate the proposed approach. Physical model evaluation was conducted in a sandbox. To ensure that the measurement results are unaffected by the surrounding air boundaries, numerical simulations were performed first to check the boundary effect. The measured apparent resistivities in the experimental set-up (sandbox with air boundaries) and that in half-space (modelled by setting side and bottom boundaries as an infinite boundary) were compared. For a soilcrete column up to 150 mm in diameter, it was found that a 1·0 m × 1·0 m × 1·0 m sand box is large enough (i.e. the maximum error of the measured apparent resistivity is found to be less than 2%, comparing to that in the half-space). ERT measurements were conducted using an AGI SuperSting R8 instrument and subsequent data were analysed using the AGI EarthImager 2D 2·4·4 (AGI, 2015) software.

In the sandbox, quartz sand (particle size ranging between 0·147 mm and 0·351 mm) with natural water content (around 3%) was used as the ground material for convenience and Portland Type I cement grout with 2 : 1 water–cement ratio was mixed to construct the soilcrete columns. The resolution of in-hole ERT is related to the soil-to-soilcrete resistivity ratio (ρ_s/ρ_{sc}). The higher the ρ_s/ρ_{sc} ratio, the better the column is resolved. In the Cyljet method, Frappin & Morey (2001) suggested $\rho_s/\rho_{sc} > 10$ is sufficient for diameter determination. The soilcrete resistivity is around 5 Ω m or less, while the quartz sand used in the sandbox experiment has a very high resistivity larger than 5000 Ω m. Owing to the large resistivity contrast, a constraint that set the maximum possible resistivity value equal to 100 000 Ω m was applied during inversion to avoid converging to unreasonable results.

In order to create the soilcrete columns in the laboratory, a large, hollow PVC tube with the target diameter and length was first fixed at the centre of the sandbox and dry sands were poured around the PVC tube until the designated height (1 m) was reached. The electrode string was then inserted into the hollow PVC tube to the designated location (approximately 10 cm above the base of sandbox). While fixing the position of the electrode string, the cement column was created by pouring the properly mixed cement grout into the PVC tube. After the cement grout had been fully poured, the PVC tube was removed from the sandbox, allowing the cement grout to flow and make contact with the surrounding sand. ERT measurement was initiated 10 min after the fresh grout had been fully placed.

Twenty-seven electrodes were deployed in both physical models with electrode spacing (s) and total spread (L) of 30 mm and 780 mm, respectively. The electrode spread was placed 100 mm away from the surface and bottom of the sandbox, in which the electrodes were installed in the fresh grout and retrieved after measurements. The electrodes adopted were stainless nut gaskets 1 mm thick and 6 mm dia. The 1 mm thick sides of these nut gaskets were aligned along the survey line to conform to the point source assumption. ERT measurements were acquired using the Wenner–Schlumberger array as in the numerical simulations, but with a total of 210 quadrupoles. The inversion scheme of physical models followed the aforementioned inversion settings of numerical simulation, in which the default values for surface ERT were used, except for two settings. The starting models were the pseudo sections while the seven iterations were set as the stopping criteria. The same resistivity inversion range from 1 to 100 000 Ω m was used in experimental data inversion.

Two physical model tests were conducted, including a uniform soilcrete column (Fig. 4(a)) and a soilcrete column with changing diameter (Fig. 4(b)). The intact soilcrete column was 75 mm in radius. The soilcrete column with changing diameter was composed of two sections, in which the radius of the upper section and the lower section is 102·5 mm and 75 mm, respectively. The same electrode spread was used for both cases. After the soilcrete columns solidified, the surrounding soils were directly excavated for visual inspection. Actual soilcrete dimensions were measured to validate the results obtained by the proposed approach.

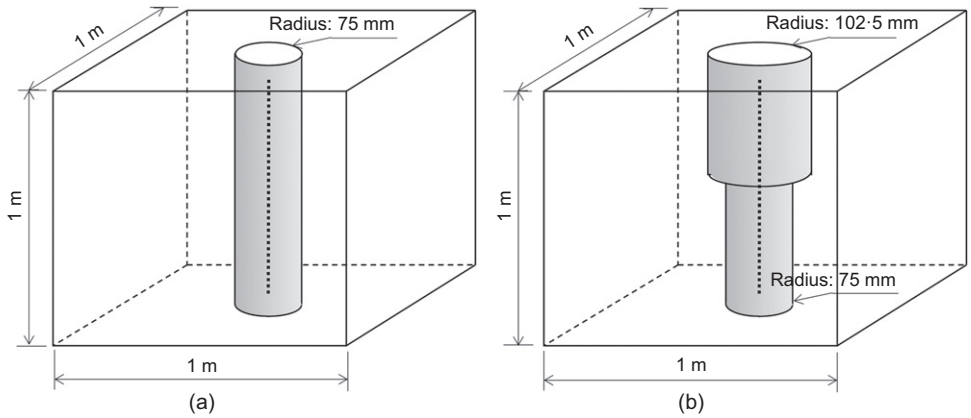

Fig. 4. Set-up of physical models in sandbox: (a) uniform soilcrete column; (b) column with changing diameter (not to scale)

RESULTS AND DISCUSSION

Similarity between axially symmetric condition and 2D Cartesian half-space

The concept of using a 2D Cartesian half-space model to perform inversion of axially symmetric in-hole data was first numerically simulated for cases of soilcrete columns with different radii. Fig. 5(a) illustrates the electrode configuration in the soilcrete column, with the dotted line indicating the 12 m long ERT survey line. The inverted results for soilcrete columns of radius 0·4 m, 0·8 m, 1·0 m and 1·2 m are shown in Figs 5(b), 5(c), 5(d) and 5(e), respectively. Results show that two distinct resistivity layers (i.e. the soilcrete and background soil) are well resolved, although close inspection reveals significant overestimation of soil resistivity. This overestimation is partly attributed to the transformation from the axially symmetric condition to 2D half-space, and is partly due to the inversion process. To further examine this problem, the synthetic apparent resistivity profile of a horizontal two-layer model is compared with that of the soilcrete column model at the centre of the measurements (i.e. the centre of the pseudo section) for the case of $r = 1{\cdot}0$ m in Fig. 6(a). It is clear that, without the top air boundary, the soilcrete column model has lower apparent resistivity at shallow depth near the electrodes. However, the apparent resistivity of the 3D soilcrete model increases much faster with depth and becomes greater than the 2D horizontal two-layer model. Both apparent resistivity profiles in Fig. 6(a) more or less increase linearly with column radius. Hence, visual determination of the soilcrete–soil interface from the apparent resistivity data is not possible.

Using the centre section of Fig. 5(d) as an example, the inverted resistivity profile (2D half-space inversion on data from soilcrete model) is compared to that of 2D inversion on data from the horizontal two-layer model (with synthetic data simulation and inversion both in 2D half-space) in Fig. 6(b). The inverted resistivity values are more reasonable in the case where forward modelling and inversion are both in the same 2D half-space condition, but there is a great deal of smoothing in the inverted resistivity profile. It is noted that the two *Y* axes have a significantly different range to plot both cases in the same figure. Not only does the 2D half-space inversion on data from the soilcrete model overestimate the soil resistivity, forcing seven iterations in the inversion, it sometimes causes an obvious resistivity drop below a certain depth. This may be explained by the low-resistivity soilcrete layer and the conversion from an axially symmetric condition to 2D half-space. Owing to the much lower resistivity in the top soilcrete layer, the percentage of current flow and measurement sensitivity in the lower half-space is drastically decreased. When converting from axially symmetric to 2D half-space, the apparent resistivity of the soilcrete model starts lower, but increases much faster with depth (column radius) and becomes greater than the horizontal two-layer model. To yield such an apparent resistivity profile as shown in Fig. 6(a), the 2D inverted resistivity in the lower half-space becomes significantly greater than its actual value (50 Ω m) because of the top low-resistivity layer. In the early stage of the study, the authors examined the inverted resistivity profile iteration by iteration, as shown in Fig. 7. Because the 3D axially symmetric condition is not really equivalent to the 2D Cartesian half-space, the

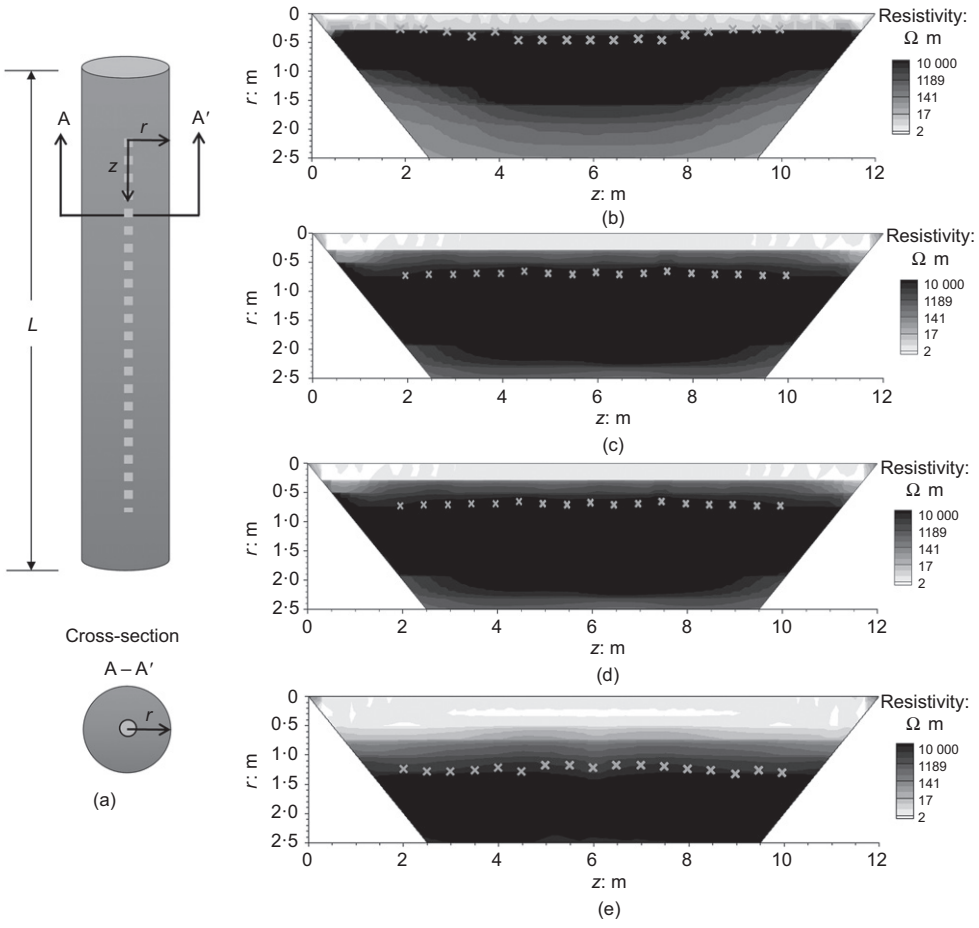

Fig. 5. Uniform soilcrete column: (a) model illustration and electrode layout; inverted resistivity sections and estimated radius plotted against depth (marked as 'x') for column radii of: (b) 0·4 m; (c) 0·8 m; (d) 1·0 m; and (e) 1·2 m

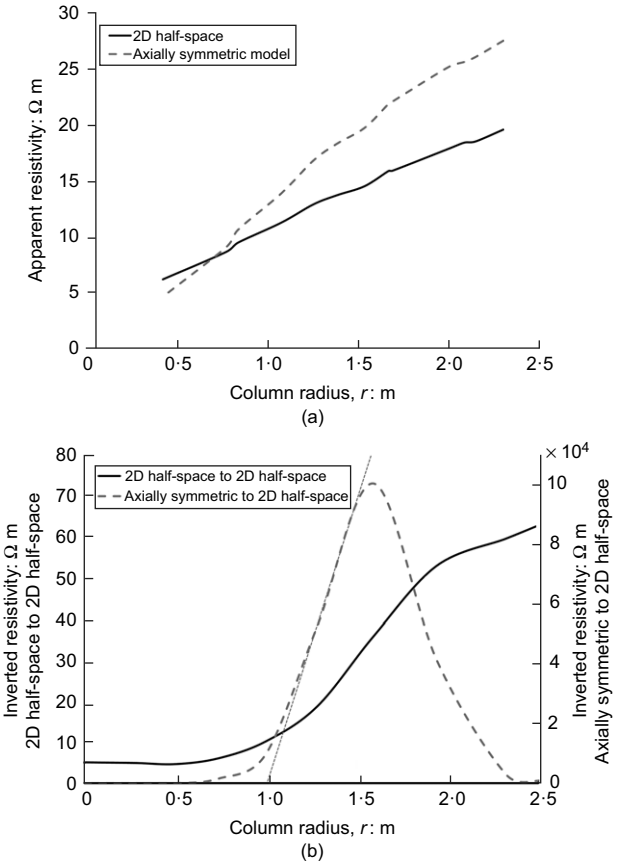

Fig. 6. Uniform soilcrete of $r = 1{\cdot}0$ m. (a) Apparent resistivity profile and (b) inverted resistivity profile at the centre ($z = 6{\cdot}0$ m), in comparison with that of two-layer model in 2D half-space

inversion cannot stop by the criterion of RMS error $<3\%$. Normally, it is stopped at iteration 3, in which the resistivity of the lower half-space is about 500 Ω m instead of the actual 50 Ω m due to the conversion from axially symmetric condition to 2D half-space. For column radius determination, the soilcrete–soil interface is still quite ambiguous in the inverted results of Figs 7(a) or 7(b). Owing to the characteristics of very-low-resistivity soilcrete over high-resistivity soil and the conversion from axially symmetric to 2D half-space, Fig. 7 shows that the grout–soil interface becomes more and more prominent when the number of iteration increases, although the resistivity below the soilcrete layer becomes unreasonably high. Iteration 7 was chosen over iteration 3 for the purpose of better quantification of the column radius.

There is also an overestimation of resistivity in the lower half-space for the 2D inversion on data from the horizontal two-layer model (with synthetic data simulation and inversion both in 2D half-space). However, the inverted resistivity here is not unrealistically high because the forward model is correct. For data generated by axially symmetric condition, the apparent resistivity deviates from the 2D half-space case, as shown in Fig. 6(a). Because the resistivity of the soilcrete layer is an order lower than that of the surrounding soil, the inverted resistivity profiles by 2D half-space (wrong forward model) becomes that shown in Fig. 7. At iteration 7, the resistivity peaks at an unrealistically high value and drops to about 800 Ω m. Although the 3D soilcrete column model is not theoretically equivalent to the horizontal two-layer model, this conversion (2D half-space inversion of 3D axially symmetric data) and high number of iterations can preserve the thickness of the first layer (column radius), and even facilitate its identification. The actual resistivity value of the background soil in the inverted profile is not important for the current purpose. The jet grouting inspection mainly concerns the actual column diameter (double the radius). Therefore, quantitative interpretation of the column diameter based on such an inversion scheme is examined as follows.

Interface interpretation from an inverted tomogram is subjective due to the smoothing regularisation in tomography inversion. As shown in Fig. 5, there is a gradual transition zone between the low-resistivity soilcrete and high-resistivity soil in the resistivity tomogram instead of a clear resistivity interface. The gradual transition blurs out the soilcrete–soil interface and leads to large uncertainty in subjective radius interpretation. Most ERT investigations delineate the interested material interface approximately by visual inspection of the colour-scaled tomograms. A more objective and accurate approach or algorithm is needed for quality control of jet grouting. Wu & Lin (2013) faced a similar problem in determining the depth of unknown foundation using ERT. Depending on the foundation type, one of the three interface delineation algorithms was found suitable, the inflection point in resistivity profile, maximum point in the transition profile and the intersection of dual tangent lines (similar to the determination of first arrival in wave propagation). Since the resistivity of the surrounding soil is highly overestimated by the 2D half-space inversion, the dual tangent line method was found to be suitable for quantitative interpretation of column radius (diameter). As illustrated in Fig. 6(b), the interface between the soilcrete column and background soil is determined by the intersection of a line tangent to the minimum point of the resistivity profile in the radial direction and the line tangent to the inflection point. The column radius corresponds to the first layer thickness in 2D half-space and the estimated values at each depth location are shown by the 'x' marks in Fig. 5. The result shows that the column radius is preserved in the layer thickness when the in-hole data are inverted by the 2D half-space model. According to the current authors' trials, keeping the same number of inversion iteration helps to reduce the uncertainty of column radius estimation. An iteration number up to 7 was used consistently throughout this study to bring the soilcrete edge to prominence, although this would cause an undue overestimation of the soil resistivity.

Figure 8 reveals the errors of column radius estimation in all cases. It shows that the accuracy of the proposed method is related to the soilcrete column radius (r) and the adopted electrode spacing (s). The electrode spacing used in the survey directly affects the spatial resolution of tomography. For $s = 0{\cdot}4$ m, as adopted in this study, the estimation error is controlled within 10% when $r \geq 1$ m. Considering that the simulation is scalable, it can be inferred from the results that a survey configuration with radius-to-spacing (r/s) ratio $\geq 2{\cdot}5$ is capable of quantifying the soilcrete radius within 10% error. In addition to the spatial resolution, the investigation radius (the depth in 2D half-space) that can be achieved by the survey line is also relevant. The radius estimation error is apparently larger at both ends of the survey line. This is attributed to the fact that fewer effective measurement data points are available at the edge of the survey line, resulting in a triangular blind zone that dips approximately 45° (Shima *et al.*, 1995), as shown in Figs 5(b)–5(e). Therefore, results within the blind zone should be excluded. From the above numerical simulation results, it appears feasible to identify the soilcrete column from surrounding soils when axially symmetric data are inverted by the 2D half-space model. Furthermore, the dual tangent line method can reasonably quantify the column radius from the inverted tomogram.

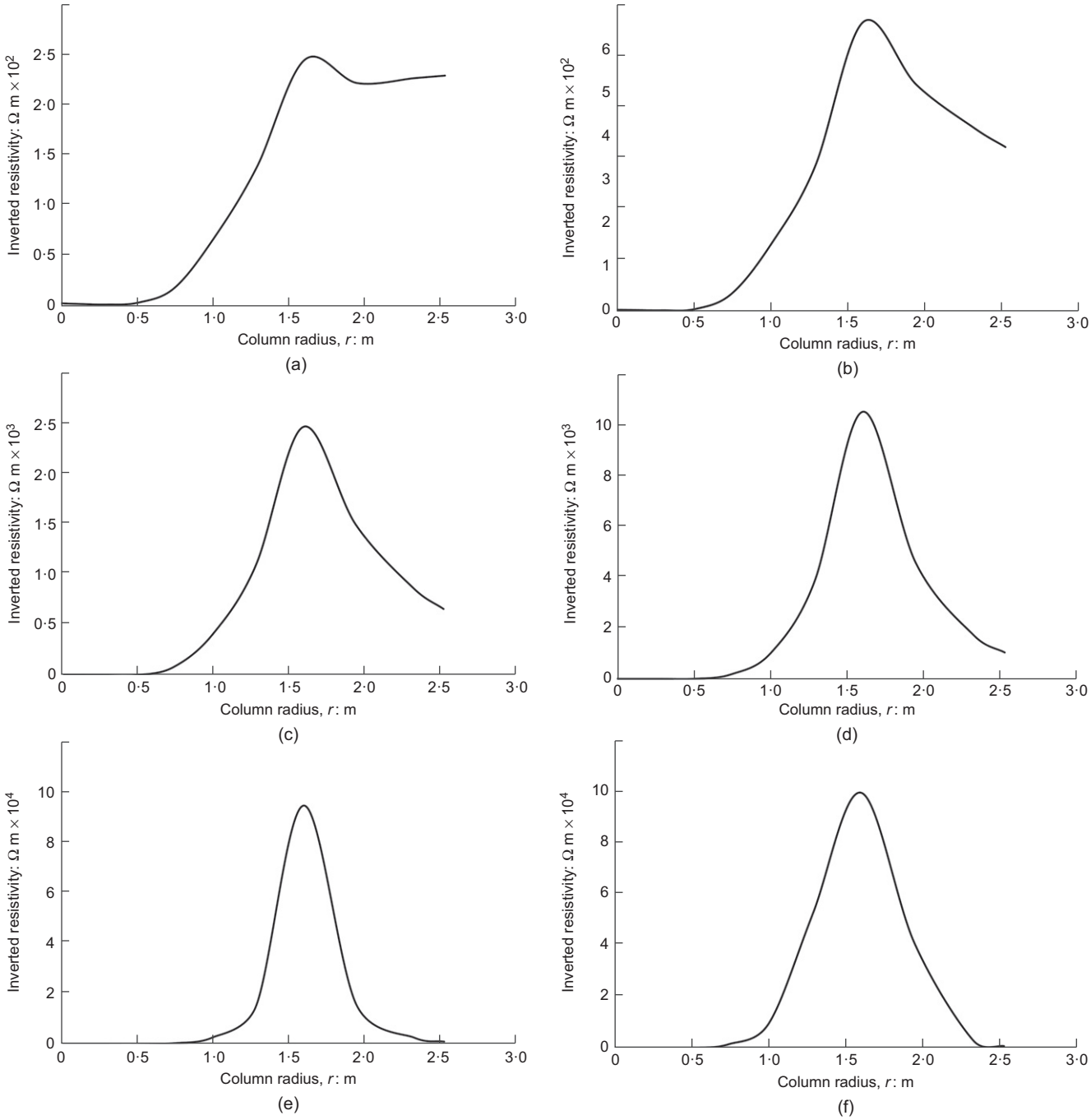

Fig. 7. Uniform soilcrete of $r = 1{\cdot}0$ m. The inverted resistivity profiles at the centre ($z = 6{\cdot}0$ m) for each iteration: (a) iteration 2 (RMS = 10·82%); (b) iteration 3 (RMS = 6·44%); (c) iteration 4 (RMS = 6·19%); (d) iteration 5 (RMS = 5·86%); (e) iteration 6 (RMS = 5·75%); (f) iteration 7 (RMS = 5·66%)

Axially symmetric defects in soilcrete column

Insufficient diameter at certain depths with a necking geometry is among the common flaws seen in jet grouting practice. It has been shown that the proposed tomography approach is able to quantify the radius (diameter) of a uniform column. Next, the ability of the proposed approach to detect axially symmetric defects is evaluated by numerical simulations. An extreme case of a discontinuous soilcrete column was first examined, in which a soilcrete column 1 m in radius has a missing (unimproved) section of different length (L_2) from 0·2 m to 1·2 m, as illustrated in Fig. 9(a). The resistivity of the missing section was set to be the same as the background soil. The inverted resistivity sections and the estimated column radius are shown in Figs 9(b)–9(e). Owing to the limited spatial resolution provided by the electrode

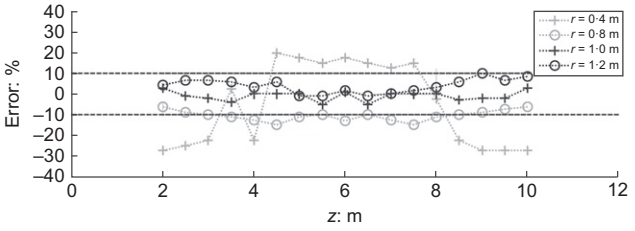

Fig. 8. Percentage errors of column radius estimation for uniform soilcrete of different radii

array and the fact that measurements are more sensitive to the low-resistivity soilcrete than high-resistivity soil, the inverted resistivity near the missing section is not identical to that in

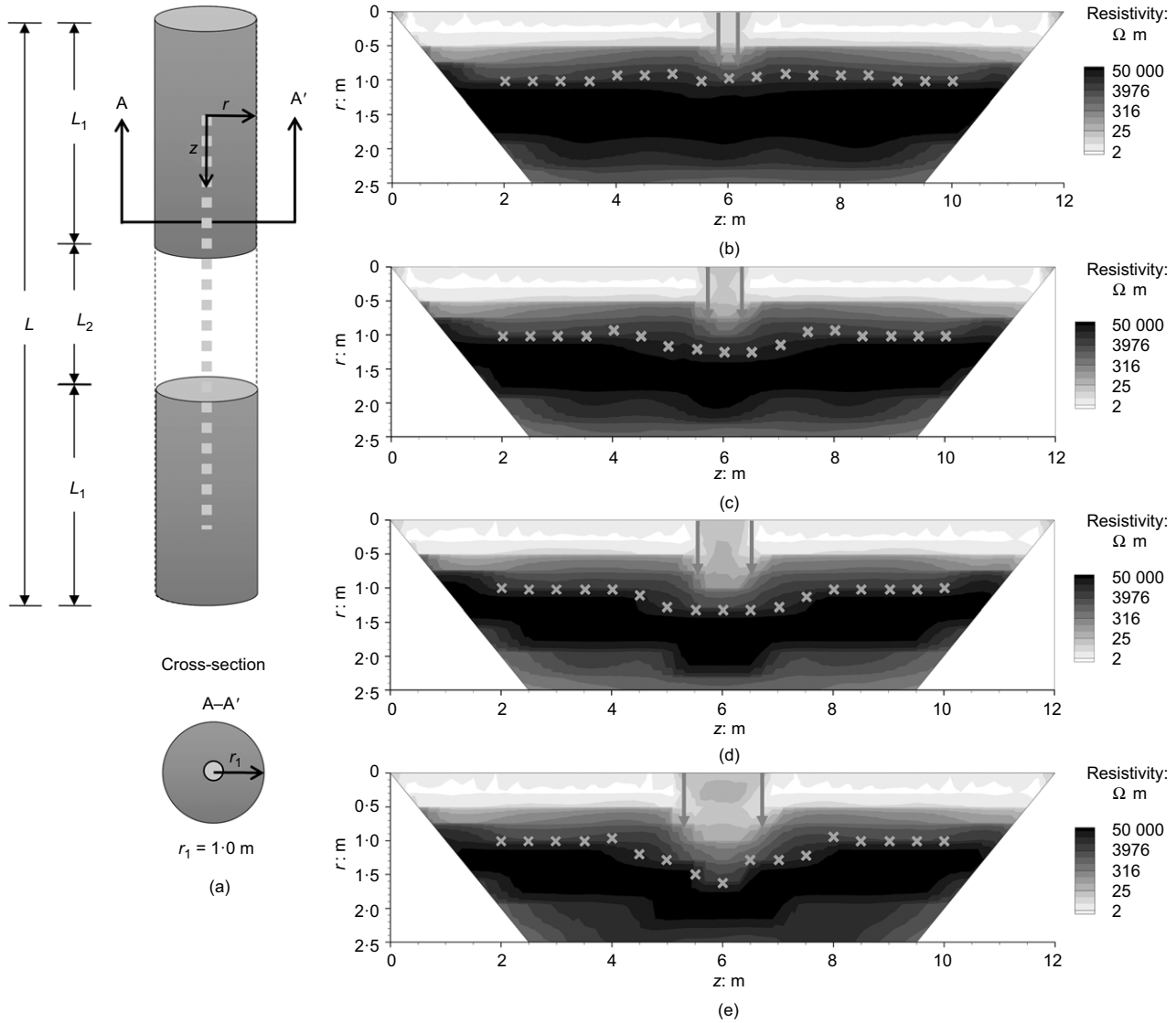

Fig. 9. Discontinuous column: (a) model schematics. Inverted resistivity sections and estimated radius plotted against depth (marked as 'x') for discontinuous length (L_2) equal to: (b) 0·2 m; (c) 0·4 m; (d) 0·8 m; and (e) 1·2 m

the background soil. Instead, the resistivity is some weighted average of soilcrete resistivity and soil resistivity. The resulting resistivity profile in the radial direction is not uniform in the missing section and the dual tangent method resulted in a radius interpretation larger than the column radius, as indicated by the cross marks in Fig. 9(b)–9(e). Therefore, Fig. 10(a) shows larger errors near the missing section on top of the old problem at both ends. A transition zone, in which the diameter estimation is less accurate, expands about one column radius above and below the missing section. Within this zone, the column radius is typically overestimated except for the low-sensitivity case where the length of the missing section is shorter than the electrode spacing.

This numerical simulation revealed the limitation of the tomography resolution. To avoid misinterpreting the missing section for a larger diameter column, a shallow high-resistivity anomaly should be regarded as a discontinuous column. In fact, it is even easier to detect a discontinuous column by examining the raw data in the form of a pseudo section. As shown in Fig. 10(b), the discontinuous section was manifested by the section of higher apparent resistivity due to the absence of low-resistivity soilcrete in the unimproved section. While the resistivity profile in the radial direction was better resolved by inversion, it seemed that the axial discontinuity of the discontinuous column was well presented in the pseudo section.

A discontinuous column is an extreme case. Under normal circumstances, the column diameter may deviate from the designed target due to geological variation or non-ideal construction control. A column with three uniform sections was used to simulate a necking soilcrete column, a simple case of an axially symmetric defect. As illustrated in Fig. 11(a), a column of 1·0 m radius has a defected necking section of 0·5 m radius and 0·2 m to 1·2 m length. The inverted resistivity sections and estimated column radius are shown in Figs 11(b)–11(e), in which the necking phenomena are clearly shown. Unlike the extreme case of a discontinuous column, no misinterpretation would be made under the necking condition. Nevertheless, it was still difficult to detect a small necking section that is shorter than the electrode spacing (as per the case shown in Fig. 11(b)) owing to insufficient spatial resolution. Due to the small radius in the necking section ($r = 0{\cdot}5$ m), which is only slightly greater than the electrode spacing, the transition in the diameter change was rather smooth in all cases and the small necking radius was not well resolved. To illustrate the effect of electrode spacing, the last case (Fig. 11(e)) was redone by reducing the electrode spacing to 0·2 m so

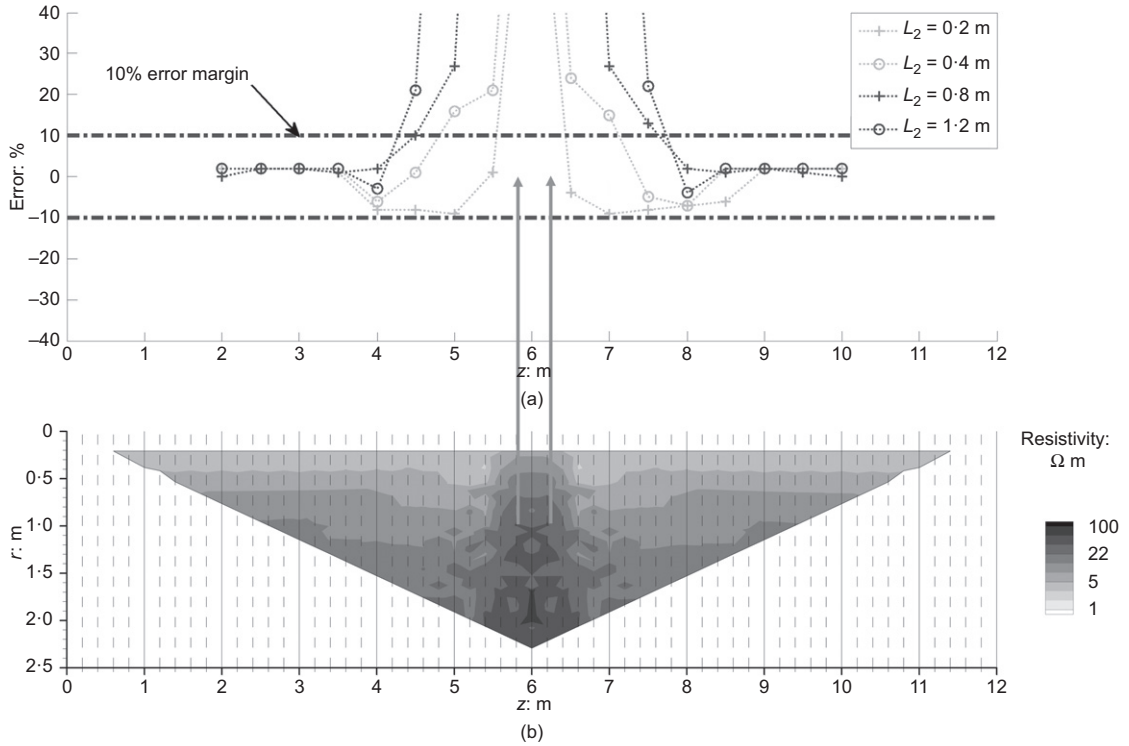

Fig. 10. Discontinuous column: (a) percentage errors of soilcrete radius estimation; (b) pseudo section of L_2 = 0·4 m corresponding to Fig. 7(c)

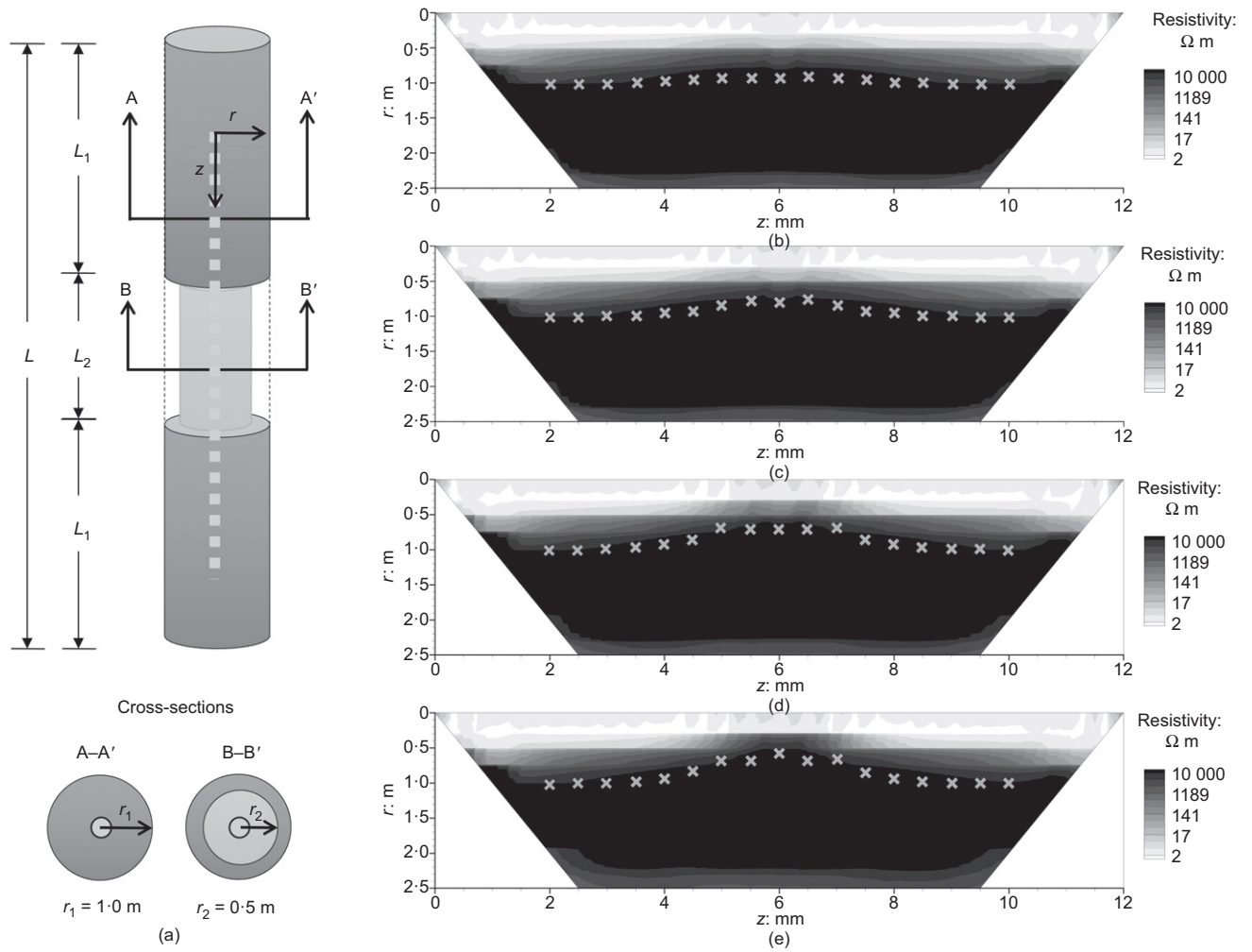

Fig. 11. Necking column: (a) model illustration. Inverted resistivity sections and estimated radius plotted against depth (marked as 'x') for necking length (L_2) equal to: (b) 0·2 m; (c) 0·4 m; (d) 0·8 m; and (e) 1·2 m

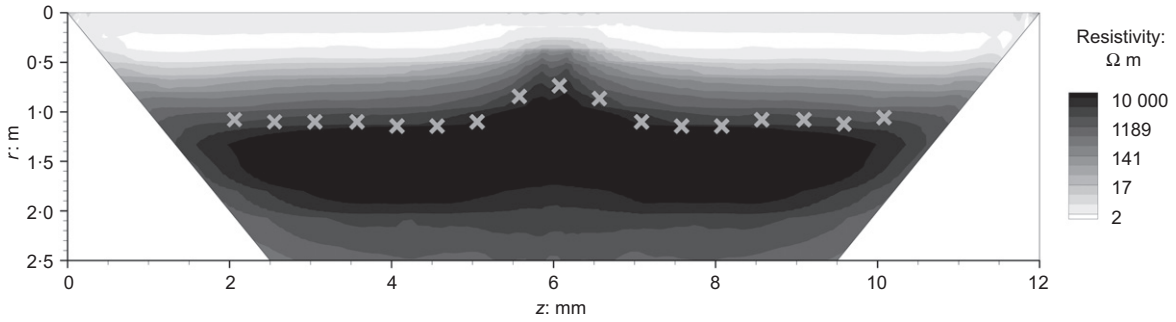

Fig. 12. Inverted resistivity sections and estimated radius versus depth (marked as 'x') for the necking column case with $L_2 = 1{\cdot}2$ m and $s = 0{\cdot}2$ m, as compared with Fig. 9(e) with $s = 0{\cdot}4$ m

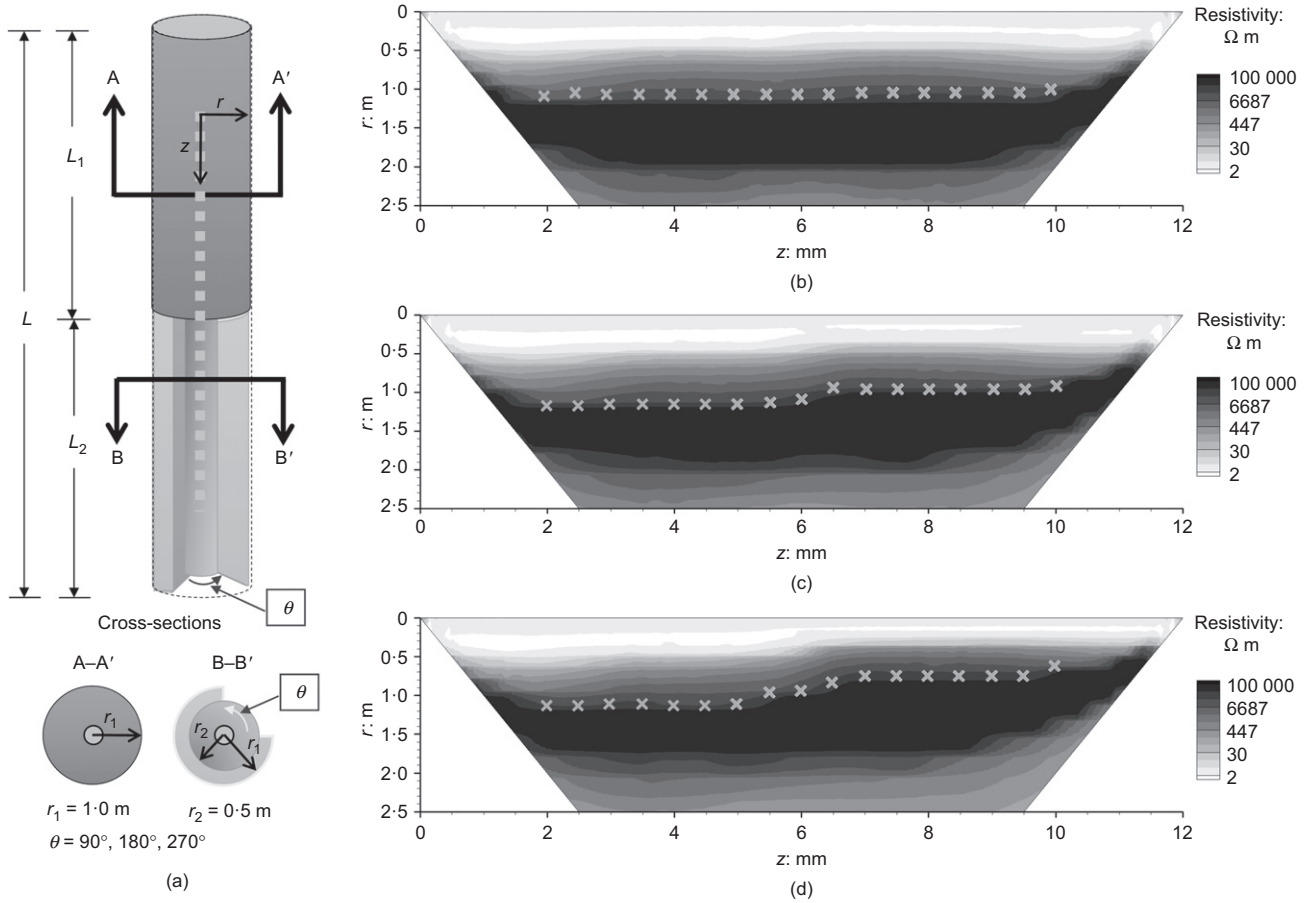

Fig. 13. Asymmetrically defective soilcrete. (a) Model illustration; (b)–(d) inverted resistivity sections with interpreted column radii

that the *r*/*s* ratio becomes 2·5 (0·5/0·2) instead of 1·25 (0·5/0·4) in the necking section. The result in Fig. 12 demonstrates that a higher *r*/*s* ratio effectively enhanced the resolution to image the change in diameter (radius) along the column. In order to detect possible anomalies and to provide a more reliable measurement profile, the *r*/*s* ratio should be predetermined for the targeted dimension, or the detection limitation arising from the selected *r*/*s* ratio should be clearly stated to prevent over-interpretation of the result.

Axially asymmetric effect on soilcrete column assessment

The axially symmetric condition can be treated as a 2D problem and analogously mapped to 2D half-space. If the soilcrete column is not axially symmetric, a 3D effect may be induced by the 2D assumption in the proposed inversion. This type of problem also arises in typical surface 2D ERT surveys when resistivity varies in the direction perpendicular to the survey line. Owing to geological variation in azimuth, the soilcrete column may not be truly circular. The 2D inverted resistivity section would reflect some weighted average from all azimuths. To examine how this axially asymmetric condition may affect the interpretation of an azimuthally averaged column radius, columns with axially asymmetric defects were simulated. As shown in Fig. 13(a), the top 6 m is a cylindrical section with 1 m radius for comparison, while the bottom 6 m is the section with axially asymmetrical defect in which the defected radius is reduced to 0·5 m in a fan-shaped region with variable arc angle θ of 90°, 180° and 270°. The inverted resistivity sections and interpreted column radii are shown in Figs 13(b)–13(e). The estimated effective radius at the defected section is 1·08 m, 0·91 m and 0·72 m for θ equal to 90°, 180° and 270°, respectively. The effective radius decreased as the cross-sectional area decreased, as expected. However, if the concept of equivalent cross-sectional area is adopted, the theoretical

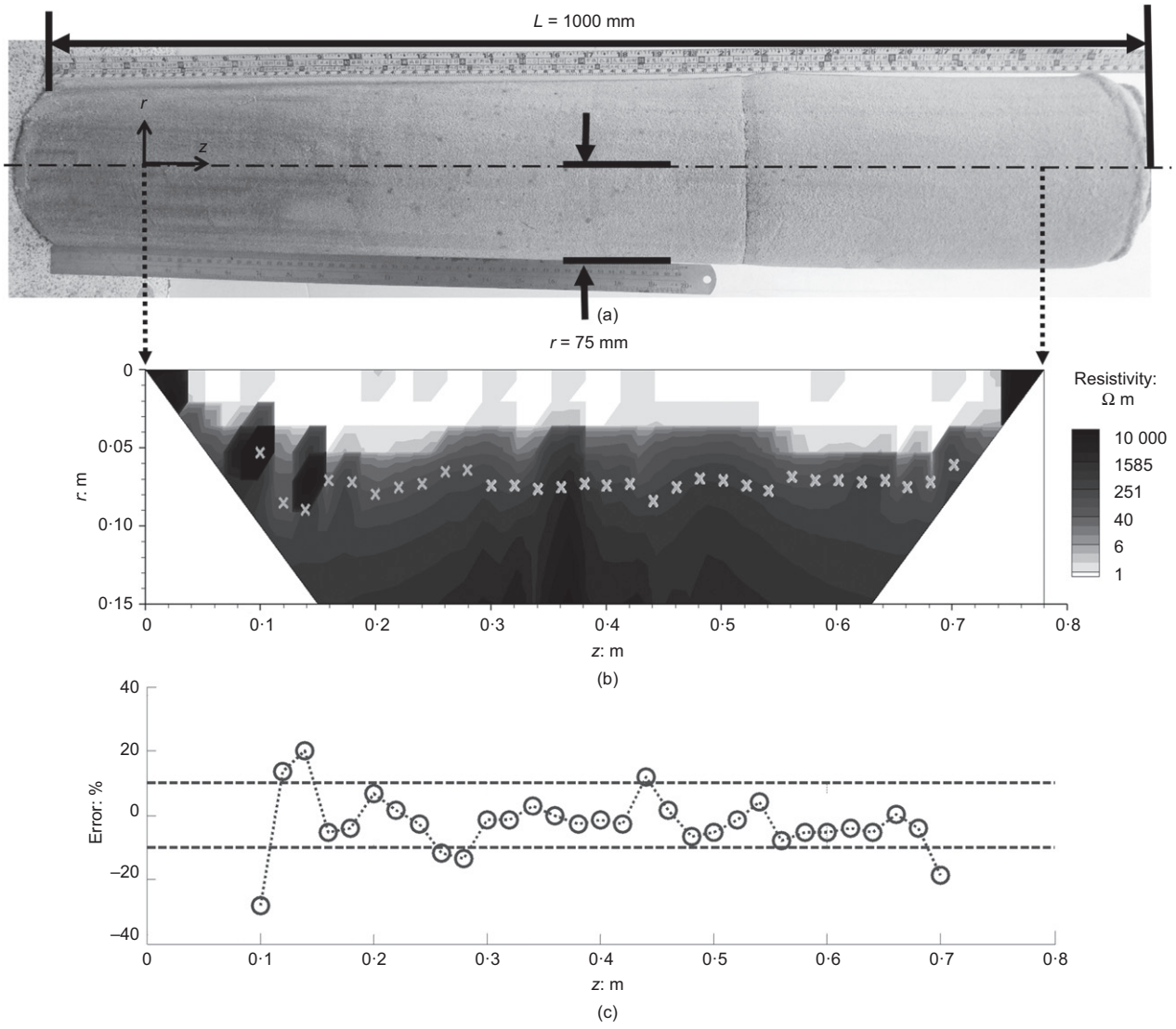

Fig. 14. Physical model test of the uniform soilcrete column. (a) Column inspection by excavation after measurement; (b) the inverted resistivity section with delineated radius; (c) corresponding percentage errors of column radius estimation

equivalent radius should be 0·90 m, 0·79 m and 0·66 m, respectively. The reduction of effective radius from measurement was not as much as what the equivalent area predicted. In the case of $\theta = 90°$ (Fig. 13(b)), the difference between the intact and asymmetrically defective section was hardly observable. As the arc angle of the reduced area increased, the reduction in the effective radius was more pronounced. These results implied that the weighting of resistivity averaging across the azimuth is not uniform. Apparently, it depends on the resistivity distribution across the azimuth. At a radius where the resistivity is not uniform azimuthally, the electrical current density concentrates more in the low-resistivity soilcrete, resulting in lower azimuthally averaged resistivity. As a result, larger effective radius was interpreted by the dual tangent line method. This result also indicated the importance of centralising the electrode string in the soilcrete column. Eccentric alignment of the electrode array may lead to non-conservative assessment of column diameter.

Physical model verification

Feasibility of the proposed in-hole ERT method has been demonstrated numerically. Physical model tests were conducted to further validate the proposed method. The experiments were performed in a sandbox in the laboratory using the aforementioned experimental set-up. The first test was a uniform soilcrete column 75 mm in radius, which was visually confirmed by excavation after hardening of the soilcrete, as shown in Fig. 14(a). The photograph was oriented 90° clockwise in Fig. 14(a) to line up with the inverted resistivity section in Fig. 14(b), in which the low-resistivity interface of the soilcrete was automatically estimated by the proposed dual tangent method (marked as 'x'). Comparing to the physical dimension of the excavated soilcrete, the error of delineated radius by in-hole ERT was mostly within 10%, as shown in Fig. 14(c).

Another soilcrete column with changing diameter was constructed in the sandbox as shown in Fig. 15(a). Direct inspection by excavation after measurement showed the top 480 mm section and the bottom 480 mm section were 102·5 mm and 75 mm in radius, respectively. The result of in-hole ERT inversion is shown in Fig. 15(b). The column diameter changed dramatically near the interface, 480 mm from the top. Both inverted resistivity images in the physical models were not as smooth as in the numerical simulations because of the large resistivity contrast between soilcrete and quartz sand, and the constraint of maximum allowable

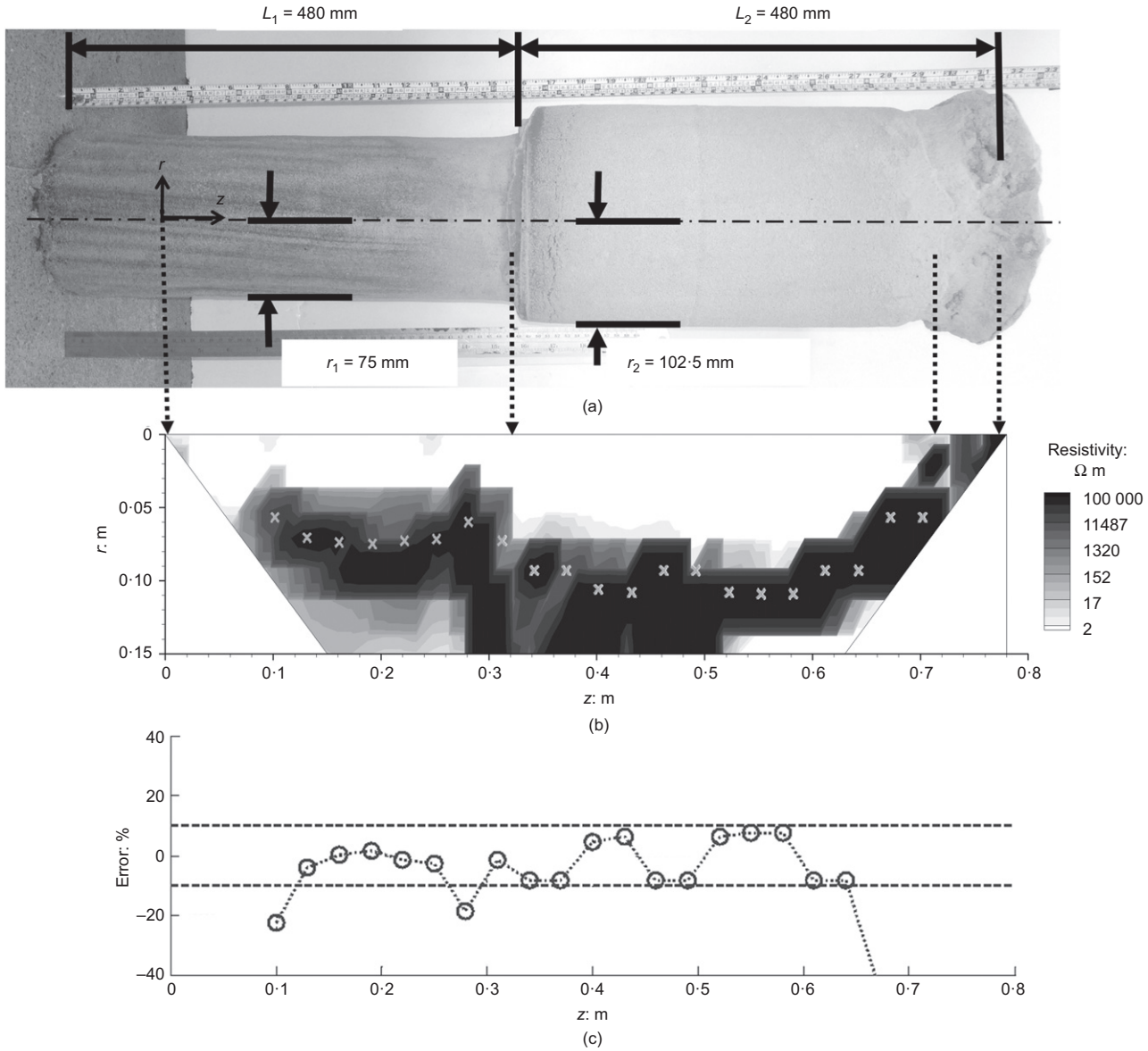

Fig. 15. Physical model test of the soilcrete column with changing diameter. (a) Column inspection by excavation after measurement; (b) the inverted resistivity section with delineated radius; (c) corresponding percentage errors of column radius estimation

resistivity during inversion. The inverted ERT section and the delineated radius from the dual tangent method (marked as 'x') are shown in Fig. 15(b) for the second case. Comparing this result to the physical dimension of excavated soilcrete, the error of delineated radius (Fig. 15(c)) is also mostly within 10%. Two measured points located at $z = 0{\cdot}7$ m had a larger error ($<-20\%$). After examining the raw data and the excavated soilcrete, the reason for this large error can be attributed to the bad coupling condition between the last two electrodes and the soilcrete. As shown in Fig. 15(a), the diameter became larger at $z = 0{\cdot}7$ m. The cement grout spread out to form a larger diameter and a cone-shaped void within the soilcrete was created. The last two electrodes were located within the void and did not function well. The measurements related to these two electrodes were filtered out prior to inversion. After re-examining the effective survey range, the performance of this case with changing diameter is also as expected. Owing to the small dimensions of the physical model, electrodes made up by stainless nut gaskets are less than ideal as point electrodes. This can partly explain why both physical models show slightly higher radius estimation error than in the numerical simulations. Other than that, the proposed approach was well supported by the two physical model tests.

CONCLUSION

In-hole electrical resistivity tomography has high potential in jet grouting dimension and integrity inspection. This study has proposed a novel approach that uses a widely available 2D Cartesian half-space inversion system to analyse the in-hole ERT data for visualisation and diameter assessment of jet grouting. Both numerical simulations and physical model tests demonstrated the feasibility of the proposed method. Owing to the similarity between the electrical potential field in a 3D axially symmetric system and a 2D Cartesian coordinate system, the inverted section reflects the geometry of the soilcrete column. The column diameter can be successfully delineated by applying the dual tangent method to the inverted resistivity profile in the radial direction when the resistivity of the surrounding soil is 10 times larger than the soilcrete. The estimation error of the column diameter is within 10% when electrode spacing is less than 1/5 of column diameter. The axial resolution in mapping the

change in diameter also depends on the electrode spacing, and the amount of necking may be underestimated if the necking section is not longer than the electrode spacing. A potential pitfall of the proposed method is the axially asymmetric effect, a type of 3D effect on a 2D assumption. The equivalent column radius is some weighted average across all azimuths, and the inverted result weighs more towards the thicker side. This finding emphasised the importance of centralising the electrode string in the soilcrete column. Eccentric alignment of the electrode array may lead to non-conservative assessment of the column diameter. The conditions of point electrode and direct coupling between electrode and soilcrete were satisfied in this study. If a slotted PVC pipe is used for electrode access, the size of slotted opening and the effect of PVC pipe should be further studied. Full-scale field testing using the proposed approach is also yet to be conducted.

ACKNOWLEDGEMENTS

Funding for this research was partly provided by the Ministry of Science and Technology under the grant no. MOST 104-2622-E-009-005-CC2 and the Environmental Protection Administration, Taiwan.

REFERENCES

AGI (Advanced Geosciences Inc.) (2015). *Instruction manual for EarthImager 2D*, version 2.4.4. Austin, TX, USA: AGI.

Arroyo, M., Gens, A., Croce, P. & Modoni, G. (2011). Design of jet-grouting for tunnel waterproofing. In *Proceedings of the 7th international symposium on the geotechnical aspects of underground construction in soft ground* (ed. G. Viggiani), pp. 181–188. London, UK: Taylor & Francis Group.

Bearce, R. G., Mooney, M. A., Niederleithinger, E. & Revil, A. (2014). Characterization of simulated soilcrete column curing using acoustic tomography. In *Geo-congress 2014 technical papers: geo-characterization and modeling for sustainability* (eds M. Abu-Farsakh, X. Yu and L. R. Hoyos), GSP 234, pp. 465–474. Reston, VA, USA: American Society of Civil Engineers.

Bearce, R. G., Mooney, M. A., Kessouri, P., Niederleithinger, E., Galindo-Guerreros, J. C. & Albers, W. (2015). Estimation of jet grout and deep soil mixed column geometry with a DC electrical resistivity push probe. *Proceedings of international symposium on non-destructive testing in civil engineering (NDT-CE)*, Berlin, Germany.

Bearce, R. G., Mooney, M. A. & Kessouri, P. (2016). Electrical resistivity imaging of laboratory soilcrete column geometry. *J. Geotech. Geoenviron. Engng* **142**, No. 3, 4015088.

Burke, G. K. (2012). The state of the practice of jet grouting. In *Grouting and deep mixing 2012* (eds L. F. Johnsen, D. A. Bruce and M. J. Byle), GSP 228, pp. 74–88. Reston, VA, USA: American Society of Civil Engineers.

Comsol Multiphysics (2013). *COMSOL Multiphysics user's guide*. Stockholm, Sweden: Comsol Multiphysics.

Croce, P. & Modoni, G. (2005). Design of jet grouting cutoffs. *Ground Improvement* **10**, No. 1, 1–9.

Croce, P., Modoni, G. & Russo, G. (2004). Jet-grouting performance in tunnelling. In *GeoSupport 2004: drilled shafts, micropiling, deep mixing, remedial methods, and specialty foundation systems* (eds J. P. Turner and P. W. Mayne), GSP 124, pp. 910–922. Reston, VA, USA: American Society of Civil Engineers.

Eramo, N., Modoni, G. & Arroyo, M. (2012). Design control and monitoring of a jet grouted excavation bottom plug. In *Proceedings of the 7th international symposium on the geotechnical aspects of underground construction in soft ground* (ed. G. Viggiani), pp. 611–618. London, UK: Taylor & Francis Group.

Flora, A. & Lirer, S. (2011). Interventi di consolidamento deiterreni, tecnologie e scelte di progetto (general report). *Proceedings of the 24th national conference on geotechnical engineering 'Innovazione tecnologica nell'ingegneria geotecnica'*, Napoli, Italy, pp. 87–148 (in Italian).

Flora, A., Modoni, G., Lirer, S. & Croce, P. (2013). The diameter of single, double and triple fluid jet grouting columns: prediction method and field trial results. *Géotechnique* **63**, No. 11, 934–945, https://doi.org/10.1680/geot.12.P.062.

Frappin, P. (2011). CYLJET – an innovative method for jet grouting column diameter measurement. In *Proceedings of the 1st international conference of engineering geophysics*, pp. 67–74. Houten, the Netherlands: European Association of Geoscientists & Engineers.

Frappin, P. & Morey, J. (2001). *Jet grouted column diameter measurement using the electric cylinder method*. Rueil-Malmaison, France: Soletanche Bachy.

Guerreros, J. C. G., Niederleithinger, E., Mackens, S. & Fechner, T. (2016). Crosshole and downhole seismics: a new quality assurance tool for jet grout columns. *Near Surf. Geophys.* **14**, No. 6, 493–501.

Hsieh, H. S., Wang, C. C. & Ou, C. Y. (2003). Use of jet grouting to limit diaphragm wall displacement of a deep excavation. *J. Geotech. Geoenviron. Engng* **129**, No. 2, 146–157.

Kimpritis, T. (2013). *The control of column diameter and strength in jet grouting processes and the influence of ground conditions*. MPhil thesis, Department of Civil and Environmental Engineering, Imperial College London, London, UK.

Liu, S. Y., Du, Y. J., Han, L. H. & Gu, M. F. (2007). Experimental study on the electrical resistivity of soil–cement admixtures. *Environ. Geol.* **54**, No. 6, 1227–1233.

Loke, M. H. (1999). *Electrical imaging surveys for environmental and engineering studies: a practical guide to 2-D and 3-D surveys*. Penang, Malaysia: M.H. Loke.

Madhyannapu, R. S., Puppala, A. J., Nazarian, S. & Yuan, D. (2010). Quality assessment and quality control of deep soil mixing construction for stabilizing expansive subsoils. *J. Geotech. Geoenviron. Engng* **136**, No. 1, 119–128.

Modoni, G. & Bzówka, J. (2012). Analysis of foundations reinforced with jet grouting. *J. Geotech. Geoenviron. Engng* **138**, No. 12, 1442–1454.

Modoni, G., Croce, P. & Mongiovì, L. (2006). Theoretical modelling of jet grouting. *Géotechnique* **56**, No. 5, 335–347, https://doi.org/10.1680/geot.2006.56.5.335.

Mooney, M. A. & Bearce, R. G. (2017). Assessment of jet grout column diameter during construction using electrical resistivity imaging. In *Grouting 2017: jet grouting, diaphragm walls, and deep mixing* (eds P. Gazzarrini, T. D. Richards Jr, D. A. Bruce, M. J. Byle, C. S. El Mohtar and L. F. Johnsen), GSP 289, pp. 42–51. Reston, VA, USA: American Society of Civil Engineers.

Niederleithinger, E., Amir, J. M. & Hübner, M. (2010). Crosshole sonic logging of secant pile walls – a feasibility study. In *23rd Symposium on the application of geophysics to engineering and environmental problems 2010 (SAGEEP 2010)*, vol. 1, pp. 685–693. Red Hook, NY, USA: Curran Associates, Inc.

Ochmański, M., Modoni, G. & Bzówka, J. (2015). Prediction of the diameter of jet grouting columns with artificial neural networks. *Soils Found.* **55**, No. 2, 425–436.

Shima, H., Kajima, K. & Kamiya, H. (1995). *Resistivity imaging profiling*. Tokyo, Japan: Kokon-shoin Publishers (in Japanese).

Spruit, R., vanTol, F., Broere, W., Slob, E. & Niederleithinger, E. (2014). Detection of anomalies in diaphragm walls with cross-hole sonic logging. *Can. Geotech. J.* **51**, No. 4, 369–380.

Tan, Y., Wei, B., Zhou, X. & Diao, Y. (2015). Lessons learned from construction of shanghai metro stations: importance of quick excavation, prompt propping, timely casting, and segmented construction. *J. Perform. Constr. Facil.* **29**, No. 4, 4014096.

Tinoco, J., Gomes Correia, A. & Cortez, P. (2016). Jet grouting column diameter prediction based on a data-driven approach. *Eur. J. Environ. Civ. Engng* **22**, No. 3, 338–358.

Wang, Z. F., Shen, S. L. & Yang, J. (2012). Estimation of the diameter of jet grouted column based on turbulent kinematic flow theory. In *Grouting and deep mixing 2012* (eds L. F. Johnsen, D. A. Bruce and M. J. Byle), GSP 228, vol. 2, pp. 2044–2051. Reston, VA, USA: American Society of Civil Engineers.

Wu, P. L. & Lin, C. P. (2013). Determining unknown bridge foundation depth using 2-dimensional electrical resistivity tomography. In *Near surface geophysics Asia Pacific conference, Beijing, China 17-19 July 2013*, pp. 197–201. Tulsa, OK, USA: Society of Exploration Geophysicists.